Retinal Pigment Epithelium Atrophy 1 (*rpea1*): A New Mouse Model With Retinal Detachment Caused by a Disruption of Protein Kinase C, θ

Xiaojie Ji, Ye Liu, Ron Hurd, Jieping Wang, Bernie Fitzmaurice, Patsy M. Nishina, and Bo Chang

The Jackson Laboratory, Bar Harbor, Maine, United States

Correspondence: Bo Chang, The Jackson Laboratory, 600 Main Street, Bar Harbor, ME 04609, USA; bo.chang@jax.org.

XJ and YL contributed equally to the work presented here and should therefore be regarded as equivalent authors.

Submitted: June 15, 2015
Accepted: January 18, 2016

Citation: Ji X, Liu Y, Hurd R, et al. Retinal pigment epithelium atrophy 1 (*rpea1*): a new mouse model with retinal detachment caused by a disruption of protein kinase c, θ. *Invest Ophthalmol Vis Sci*. 2016;57:877–888. DOI:10.1167/iovs.15-17495

Purpose. Retinal detachments (RDs), a separation of the light-sensitive tissue of the retina from its supporting layers in the posterior eye, isolate retinal cells from their normal supply of nourishment and can lead to their deterioration and death. We identified a new, spontaneous murine model of exudative retinal detachment, *nm3342* (new mutant 3342, also referred to as *rpea1*: retinal pigment epithelium atrophy 1), which we characterize herein.

Methods. The chromosomal position for the recessive *nm3342* mutation was determined by DNA pooling, and the causative mutation was discovered by comparison of whole exome sequences of mutant and wild-type controls. The effects of the mutation were examined in longitudinal studies by clinical evaluation, electroretinography (ERG), light microscopy, and marker and Western blot analyses.

Results. New mutant 3342, *nm3342*, also referred to as *rpea1,* causes an early-onset, complete RD on the ABJ/LeJ strain background, and central exudative RD and late-onset RPE atrophy on the C57BL/6J background. The ERG responses were normal at 2 months of age but deteriorate as mice age, concomitant with progressive pan-retinal photoreceptor loss. Genetic analysis localized *rpea1* to mouse chromosome 2. By high-throughput sequencing of a whole exome capture library of an *rpea1/rpea1* mutant and subsequent sequence analysis, a splice donor site mutation in the *Prkcq* (protein kinase C, θ) gene, was identified, leading to a skipping of exon 6, frame shift and premature termination. Homozygotes with a *Prkcq*-targeted null allele ($Prkcq^{tm1Litt}$) have similar retinal phenotypes as homozygous *rpea1* mice. We determined that the PKCθ protein is abundant in the lateral surfaces of RPE cells and colocalizes with both tight and adherens junction proteins. Phalloidin-stained RPE whole mounts showed abnormal RPE cell morphology with aberrant actin ring formation.

Conclusions. The homozygous $Prkcq^{rpea1}$ and the null $Prkcq^{tm1Litt}$ mutants are reliable novel mouse models of RD and can also be used to study the effects of the disruption of PRKCQ (PKCθ) signaling in RPE cells.

Keywords: retinal detachment (RD), retinal pigmented epithelium (RPE), protein kinase C, theta (PKCθ), spontaneous mutation

The cellular layers in the posterior eye, including the RPE, choroid, and sclera, support the overlying neuroretina to enable proper vision. Their supportive functions include, but are not limited to, recycling of chromophores, providing nutrients, exchanging fluid and waste products, and serving barrier and structural functions. Not surprisingly, therefore, separation of the neuroretina from these supportive structures, termed retinal detachment (RD), can lead to significant visual defects, and in some cases, if left untreated, to permanently impaired vision or total blindness. Retinal detachments can result from trauma, postsurgical complications, or inflammatory eye disorders and are a symptom of diseases, such as myopia, glaucoma, Stickler's syndrome, eclampsia, and others.[1–3] It is also associated with common retinal vascular diseases such as persistent fetal vasculature, retinopathy of prematurity, and ischemic and familial proliferative vitreoretinopathy,[4,5] and in older individuals, proliferative diabetic retinopathy[6] and secondary epiretinal membranes.[7]

Retinal detachments are generally classified as rhegmatogenous, exudative (serous), or tractional. Rhegmatogenous RDs occur as a result of a break in the retina that allows vitreal fluid to pass into and accumulate in the subretinal space. Exudative RDs develop in the absence of a retinal break but also result in fluid accumulating between the retina and RPE. Tractional RDs are caused by fibrous or fibrovascular tissue that pull the neuroretina from the RPE. The population frequency of RDs is not readily available. However, a review of published studies from 1970 through 2009 by Mitry et al.[8] showed that the rate of rhegmatogenous retinal detachments ranged from 6.3 to 17.9 per 100,000 and that the median annual incidence in those studies that reported a sample size >300 was 10.5. Hence, it is likely, that when all classes of RD are accounted for, a fair number of ophthalmically compromised individuals have this malady.

Although some of the causative factors for the development of RDs have been identified, the mechanisms underlying the pathology are largely unknown. For example, although serous or exudative RD is associated with inflammatory, infectious,

Investigative Ophthalmology & Visual Science

vascular, degenerative, malignant, or genetically determined pathologic conditions that lead to an imbalance of ocular fluid inflow and outflow, how that imbalance occurs and the molecules involved need to be further defined. Alterations in the choroidal vascular permeability and interstitial fluid composition, as well as defects in RPE adhesion that lead to changes in barrier permeability, have been reported to contribute to the exudative retinal detachments.[9,10] To understand what factors lead to these alterations and the mechanisms underlying the disease, an animal model that reproducibly develops RD would be extremely useful.

A new mouse mutation, *nm3342*, causing exudative RD, was discovered in the ABJ/LeJ inbred strain by the Eye Mutant Resource (EMR; Bar Harbor, ME, USA) screening program and was subsequently moved onto the C57BL/6J background. In a longitudinal characterization of the model, we determined that the *nm3342* mutation on the C57BL/6 background leads to both central RD, which appears to be exudative in nature as no neuroretinal breaks are observed by indirect ophthalmoscopy, optical coherence tomography (OCT), or histology, and to RPE atrophy. We therefore renamed this model retinal pigment epithelium atrophy 1 (*rpea1*). The homozygous B6.ABJ-*rpea1* mice have a normal electroretinography (ERG) at 2 months of age, but the amplitudes of rod a- and b-waves diminish thereafter, corresponding to progressive photoreceptor loss, as assessed by histology. Through linkage analysis and high-throughput sequencing, we identified a nonsense mutation in the *Prkcq* gene, which encodes protein kinase C, θ (PKCθ). Henceforth, *nm3342* will be referred to as *Prkcq*^{rpea1} or *rpea1*. The model also exhibits early abnormalities in RPE cortical actin formation, progressive photoreceptor degeneration, and late-onset focal regions of RPE atrophy.

Protein kinase C, θ has been studied mainly in respect to T-cell activation.[11] However, in other cell types, PKCθ has been suggested to play a role in cell adhesion and in establishing neuronal cell polarity.[12,13] Further study of this model, *Prkcq*^{rpea1}, will provide entry points into understanding how this signaling molecule functions to maintain fluid homeostasis in the posterior eye.

Materials and Methods

Mice

The mice in this study were bred and maintained in standardized conditions of the Production and Research Animal Facilities at The Jackson Laboratory (JAX; Bar Harbor, ME, USA). They were provided with an NIH31 6% fat chow diet and acidified water, in a pathogen-free vivarium environment with a 14-hour light/10-hour dark cycle. All experiments were approved by the Institutional Animal Care and Use Committee and conducted in accordance with the ARVO Statement for the Use of Animals in Ophthalmic and Vision Research.

Origin

The *rpea1* was discovered in the inbred mouse strain ABJ/LeJ, which exhibited a star-shaped fundus pattern. Each arm of the star corresponded to a retinal blood vessel, and it appeared that the retina detached and folded along the length of both veins and arteries. The interpretation of the disease phenotype was complicated because the RD phenotype spontaneously arose in the ABJ/LeJ strain that carries two other mutations: asebia in stearoyl-coenzyme A desaturase 1 (*Scd1*$^{ab\text{-}J}$) and retinal degeneration 1 in phosphodiesterase 6b (*Pde6b*^{rd1}). To test for the possibility of a new mutation causing RD, mice from this strain were mated to C57BL/6J mice, which have a normal retina. The F1 progeny, which did not show ocular abnormalities, were intercrossed. The intercrossed (F2) offspring could be separated into different groups by fundus examination. Two groups were selected to continue backcross to C57BL/6J for five generations. Mice from group 1 exhibited patches of depigmentation and were developed as a new strain, B6.ABJ-*Prkcq*^{rpea1}/BOC (stock #004658), which only carried the *rpea1* mutation. Mice from group 2 exhibited a star-shaped fundus pattern and were developed as a new strain, B6.ABJ- *Prkcq*^{rpea1}*Pde6b*^{rd1}/BOC (stock #018777), which carried the *rpea1* and *rd1* mutations.

Clinical Evaluation and Electroretinography

Eyes of all mice used in the characterization studies and linkage crosses were dilated with 1% atropine ophthalmic drops (Bausch and Lomb Pharmaceuticals, Inc., Tampa, FL, USA) and were evaluated by indirect ophthalmoscopy with a 78-diopter lens. Fundus photographs were taken with a Kowa small animal fundus camera using a Volk superfield lens held 2 inches from the eye as previously described[14] or with a Micron III in vivo bright-field retinal imaging microscope equipped with image-guided OCT capabilities (Phoenix Laboratories, Inc., Pleasanton, CA, USA).

For ERG evaluation of mutants, following an overnight dark adaptation, mice were anesthetized with an intraperitoneal injection of xylazine (80 mg/kg) and ketamine (16 mg/kg) in normal saline. Additional anesthetic was given if akinesia was inadequate. The equipment and protocol used here were as previously described.[15] Briefly, dark-adapted, rod-mediated ERGs were recorded with the responses to short-wavelength flashes over 4.0-log units to the maximum intensity by the photopic stimulator. Cone-mediated ERGs were recorded with white flashes after 10 minutes of complete light adaptation. The signals were sampled at 0.8-ms intervals and averaged.

Histologic Analysis

Mice were asphyxiated by carbon dioxide inhalation, and enucleated eyes were fixed overnight in cold methanol/acetic acid solution (3:1, vol/vol). The paraffin-embedded eyes were cut into 6-μm sections, stained with hematoxylin and eosin, and examined by light microscopy.

Gene Mapping and Sequencing

To determine the chromosomal location of the *rpea1* gene, we mated B6.ABJ-*rpea1* mice to CAST/EiJ mice. The F1 mice, which did not exhibit retinal abnormalities, were intercrossed to produce F2 mice. Tail DNA was isolated as previously reported.[16] A genome-wide scan of pooled DNA from 12 affected and 12 unaffected mice was carried out using 48 microsatellite markers.[17] The discoloration of the fundus cosegregated with markers on chromosome 2. Subsequently, DNAs of 54 F2 offspring with the *rpea1* phenotype from a (B6.ABJ-*rpea1* × CAST/EiJ) F1 intercross were genotyped using microsatellite markers to develop a fine structure map of the chromosome 2 region. Microsatellite markers *D2Mit75, D2Mit3, D2Mit118, D2Mit360*, and *D2Mit6* were scored on individual DNA samples. For PCR amplification, 25 ng DNA was used in a 10-μL volume containing 50 mM KCl, 10 mM Tris-HCl, pH 8.3, 2.5 mM $MgCl_2$, 0.2 mM oligonucleotides, 200 μM dNTP, and 0.02 U AmpliTaq DNA polymerase. The reactions were initially denatured for 3 minutes at 94°C and then subjected to 40 cycles of 15 seconds at 94°C, 1 minute at 51°C, 1 minute at 72°C, and then a final 7-minute extension at 72°C. The PCR products were separated by electrophoresis on 3% MetaPhor

Investigative Ophthalmology & Visual Science

(FMC, Rockland, ME, USA) agarose gels and visualized under UV light after staining with ethidium bromide.

The causative mutation was discovered by comparing the whole exome sequences from a homozygous *rpea1* mutant and control.[18] To confirm the detected variant by Sanger sequencing, we designed one pair of PCR primers to amplify a cDNA fragment from exon 4 to exon 8 of the *Prkcq* gene. For direct sequencing, the PCR reaction was scaled up to 30 μL; amplification was done for 36 cycles with a 15-second denaturing step at 94°C, a 2-minute annealing step at 60°C, and a 2-minute extension step at 72°C. Teh PCR products were purified from agarose gels using a Qiagen kit (Qiagen, Germantown, MD, USA). Sequencing reactions were carried out with automated fluorescence tag sequencing. Total RNA was isolated from retinas of *rpea1* mutant mice by TRIZOL LS reagent (GIBCO BRL; Waltham, MA, USA), and the SuperScriptTM preamplification system (GIBCO BRL) was used to make first-strand cDNA. The following primer pair was used to amplify the cDNA fragment and sequence directly: *Prkcq*-1F: CTCAAGGCC GAATGCTAATG; *Prkcq*-1R: ACAGTGCTCACAGAAGGTTG.

Antibodies

Mouse antibody to PKCθ (IgG2a; #610090; BD Biosciences; San Jose, CA, USA), rabbit ZO-1 antibody (61-7300; Invitrogen, Carlsbad, CA, USA), mouse β-catenin antibody (IgG1; #sc-7963; Santa Cruz Biotech; Dallas, TX, USA), mouse antibody to ezrin (E8897; Sigma-Aldrich Corp., St. Louis, MO, USA), goat antibody to ezrin (sc-6409; Santa Cruz Biotech), rabbit antibody to glial fibrillary acidic protein (GFAP; DAKO, Carpinteria, CA, USA), mouse antibody to moesin/radixin (ab50007; Abcam, Cambridge, MA, USA), rabbit antibody to radixin (ab52495; Abcam), mouse antibody to rhodopsin (MS-1233-R7; Thermo Scientific, Waltham, MA, USA), rabbit antibody to blue opsin (AB5407; Chemicon International, Billerica, MA, USA), rabbit antibody to red/green opsin (AB5405; Millipore, Billerica, MA, USA), mouse antibody to E-cadherin (610181; BD Transduction, San Jose, CA, USA), rabbit antibody to pan-cadherin (ab6529-200; Abcam), rabbit antibody to α1 catenin (2028-1; Epitomics, Burlingame, CA, USA), rabbit phospho-ezrin/radixin/moesin (ERM) antibody (#3149; Cell Signaling, Danvers, MA, USA), and rabbit occludin antibody (#71-1500; Invitrogen) were used for marker analyses of the mutant. The loading control sampler kit (#4670; Cell Signaling) included horseradish peroxidase (HRP)-conjugated β-tubulin, β-actin, and glyceraldehyde-3-phosphate dehydrogenase (GAPDH) antibodies.

Preparation and Retinal Adhesion Measurement

To assess retinal adhesion, a protocol described by Nandrot et al.[19] was utilized. Three-week-old C57BL/6J and *Prkcq*$^{rpea1/rpea1}$ mice were asphyxiated with CO_2 2 hours after the onset of the light cycle. The anterior segment was quickly removed from each enucleated eye in HEPES-buffered Hanks' saline solution containing calcium and magnesium. Following a single radial cut toward the optic nerve, the neural retina was gently peeled from the underlying tissue. The dissection was performed at room temperature. The peeled-off neural retina was then flattened facing upward on a glass slide for viewing with bright-field microscopy.

For protein preparation, the separated neural retina or whole eyecups were homogenized in ice-cold lysis buffer (50 mM Tris-HCl, pH 8.0, 1 mM EDTA, 150 mM NaCl, 1% NP-40, 0.1% SDS, and 0.5% sodium deoxycholate, freshly supplemented with 100 mM sodium orthovanadate, 10 mM ammonium molybdate, 0.2 M sodium pyrophosphate, 1 M NaF, 0.1 M phenylmethanesulfonyl fluoride, and 1% of protease inhibitor cocktails; EMD Millipore). Protein representing 10% of one mouse retina or whole eyecup was mixed with reducing sample buffer and separated on 10% SDS-polyacrylamide gels. After transfer to nitrocellulose membrane and blocking with 5% nonfat milk in TBST (0.9% NaCl, 100 mM Tris, 0.05% Tween-20, pH 7.4), the blots were incubated with primary antibodies to ezrin, GFAP, and β-tubulin and with appropriate HRP-conjugated secondary antibodies, followed by chemiluminescence detection (Supersignal West Pico Chemiluminescent Substrate [Pierce, Rockford, IL, USA] for ezrin and by Luminata Classico Western HRP Substrate [Millipore Corporation] for GFAP and β-tubulin). Western blot bands were quantified by densitometry measurement using Fiji software.

Preparation and Immunostaining of RPE Flat Mounts

After enucleation, mouse eyes were punctured with a fine needle and immersion fixed in ice-cold 10% neutral-buffered formalin (NBF) for 10 minutes. The anterior segment was removed, and the neural retina was separated from the RPE-choroid-sclera. Six radial cuts were made toward the optic nerve to flatten the posterior eyecup. After total fixation of 30 minutes in NBF, the tissue was washed three times with PBS, incubated with PBST (PBS with 0.1% Tween-20) for 20 minutes, and blocked with 5% goat serum in PBST for 30 minutes. For phalloidin staining, tissues were incubated with Alexa Fluor 488-phalloidin (1:300; Invitrogen) in blocking solution overnight at 4°C; for double staining, tissues were incubated with ZO-1 antibody (1:300 dilution) in blocking solution overnight at 4°C, washed with PBST, and incubated with Alexa Fluor 555–conjugated goat anti-rabbit antibody (1:200; Invitrogen) and Alexa Fluor 488 phalloidin (1:300; Invitrogen) for 2 hours. Nuclei were stained by incubating with 4′,6-diamidino-2-phenylindole (DAPI) for 20 minutes. The whole RPE-choroid-sclera tissue was then flat mounted, with RPE side up, onto slides and cover-slipped for imaging. Fluorescent images were captured with a Leica SP5 confocal microscope (Leica Microsystems, Buffalo Grove, IL, USA), and identical imaging parameters were applied to both WT and mutant RPE flat mounts.

Immunohistochemistry

Mouse eyes were enucleated and immersion fixed in acetic methanol (for ezrin, PKCθ, ZO-1, rhodopsin, PNA [peanut agglutinin], blue opsin, red/green opsin) or 4% paraformaldehyde (for ezrin, moesin/radixin, radixin, E-cadherin, pan-cadherin, α1 catenin, PKCθ, and β-catenin) for 1 hour, dehydrated, and embedded in paraffin. Seven-micrometer-thick sections were cut, deparaffinated, rehydrated, and microwave heated in antigen retrieval buffer (10 mM Tris-HCl, 2 mM EDTA, 0.01% Tween-20, pH 9.5). Sections were then blocked with 4% goat serum in PBST, followed by primary antibody incubation at 4°C overnight. For PKCθ and ZO-1 coimmunostaining, fluorescent detection was performed with Alexa Fluor 555–conjugated goat anti-mouse and Alexa Fluor 488–conjugated goat anti-rabbit secondary antibodies (Invitrogen). For PKCθ and β-catenin coimmunostaining, Cy3-goat anti-mouse IgG2a (Jackson ImmunoResearch Labs, Bar Harbor, ME, USA), and Alexa Fluor 488-goat anti-mouse IgG1 (Invitrogen) were used to detect PKCθ and β-catenin, respectively. For PNA and cone opsin staining, sections were coincubated with biotinylated PNA (Vector Laboratories, Burlingame, CA, USA) and Cy3-donkey anti-rabbit IgG (Jackson ImmunoResearch Labs) for 2 hours at room temperature, followed by 30-minute incubation with fluorescein-conjugated avidin D (Vector Laboratories). Peanut agglutinin/blue opsin figures were taken from ventral

Investigative Ophthalmology & Visual Science

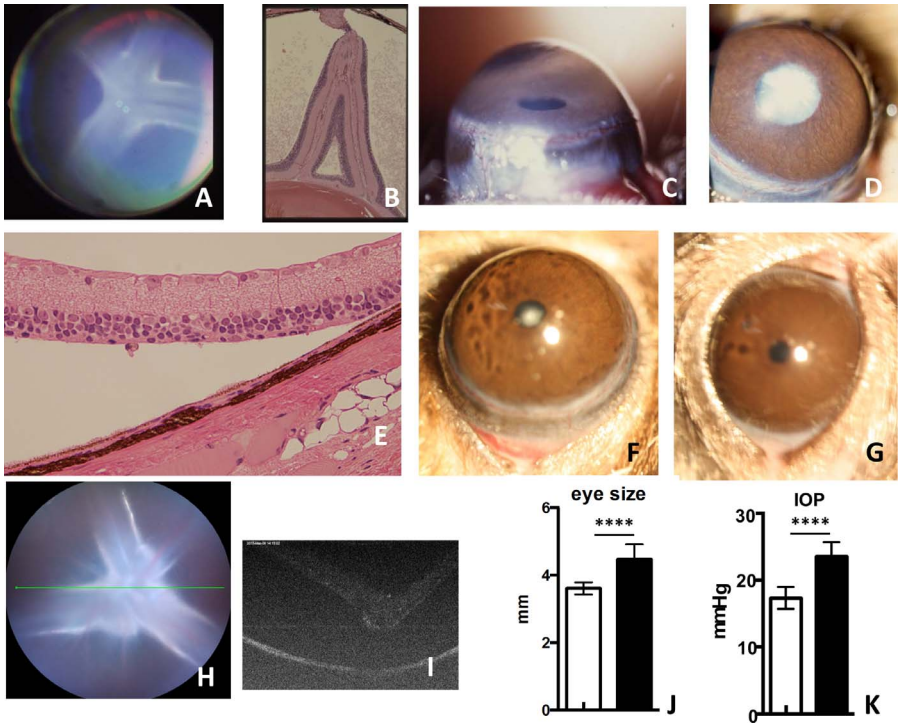

Figure 1. ABJ/LeJ ocular phenotypes (**A–E**). (**A**) Star-shaped pattern observed by fundus examination at 1 month of age. (**B**) Histologic sections indicate that the star-shaped pattern corresponds to a complete RD. (**C**) Protuberant eye. (**D**) Cataract. (**E**) Photoreceptor and ganglion cell loss in the mice at 6 months of age. GC, ganglion cell; IPL, inner plexiform layer; INL, inner nuclear layer; CH, choroid. *Scale bar*: 10 μm. B6.ABJ-*Prkcq*^{rpea1}*Pde6b*^{rd1}/BOC phenotypes (**F–K**). (**F**) Enlarged and (**G**) normal size eye, (**H**) retinal star, and (**I**) complete RD. The eye size (**J**) (*white bar*, control mice = 3.63 ± 0.17 mm and *black bar*, mutant mice = 4.47 ± 0.47 mm; ****statistically significant at $P < 0.0001$) and IOP (**K**) (*white bar*, control mice = 17.3 ± 1.7 mm Hg and *black bar*, mutant mice = 23.5 ± 4.5 mm Hg; ****statistically significant at $P < 0.0001$) at 3 months of age.

region of eyecups, and PNA/red opsin figures were taken from dorsal region of eyecups. DAPI was used for nuclear counterstain. Fluorescent images were captured by confocal microscopy with identical imaging conditions applied to both wild-type (WT) and mutant sections.

Western Blotting

Whole eyes were enucleated and placed in ice-cold Dulbecco's phosphate-buffered saline (Invitrogen). Extraneous tissue adhering to the eye globe was trimmed away, and anterior segments were removed. The neural retina was separated from the RPE-choroid-sclera, and both tissues were immediately frozen in liquid nitrogen. For RPE-choroid lysate preparation, the RPE-choroid-sclera tissues from both eyes of a mouse were gently homogenized using a glass Teflon homogenizer in 170 mL ice-cold lysis buffer (25 mM Tris-HCl, pH 7.2, 150 mM NaCl, 5 mM $MgCl_2$, 1% NP-40, and 5% glycerol, supplemented with complete EDTA-free, proteinase inhibitor and PhosSTOP phosphatase inhibitor cocktail; Roche, Indianapolis, IN, USA), until the sclera became clear. The RPE-choroid lysates were then centrifuged at 12,000*g* for 5 minutes at 4°C, and the supernatants were collected. Protein concentration was determined using the Bradford Ultra kit (Expedeon). Equal amounts of lysate protein were fractionated by SDS-PAGE and transferred to a polyvinylidene difluoride membrane using standard protocols (Bio-Rad, Hercules, CA, USA). After blocking with 4% nonfat milk in TBST (137 mM sodium chloride, 20 mM Tris, and 0.05% Tween-20, pH 7.5), the blots were incubated with the indicated primary antibodies diluted in 4% BSA in TBST and detected with either an anti-mouse or anti-rabbit HRP-conjugated secondary antibody (Bio-Rad) diluted 1:2000 in 4% nonfat milk (TBST). Signals were developed using Supersignal West Pico Chemiluminescent Substrate (Pierce). Western blot bands were quantified by densitometry using ImageJ software (http://imagej.nih.gov/ij/; provided in the public domain by the National Institutes of Health, Bethesda, MD, USA [gel analysis tool]), and the signals of the target protein were normalized to that of β-tubulin.

Statistics

Results are represented as mean ± SD. Statistical significance was determined by unpaired *t*-tests; $P < 0.05$ was considered statistically significant.

Results

Complete RD and Other Ocular Abnormalities in *nm3342* Mutants on the ABJ/LeJ and C57BL/6J Background

New mutant 3342, *nm3342*, was first identified by indirect ophthalmoscopy as a bilateral star-shaped fundus pattern in an ABJ/LeJ mouse (Fig. 1A). The star pattern was lost when the mutant was held upside down and reappeared when the mouse was held upright. Each arm of the star was associated with a retinal blood vessel; the detached retina appeared to fold down along the vessels. The retinal star was observable by 1 month of age. Histologic sections document a complete retinal detachment (Fig. 1B). By 6 months of age, all ABJ/LeJ mice had enlarged eyes (Fig. 1C) with high intraocular pressure (IOP) levels (not shown), cataracts (Fig. 1D), and ganglion and photoreceptor cell loss (Fig. 1E). In congenic B6.ABJ-*Prkcq*^{rpea1}*Pde6b*^{rd1}/BOC mice, which carried the *rpea1* and

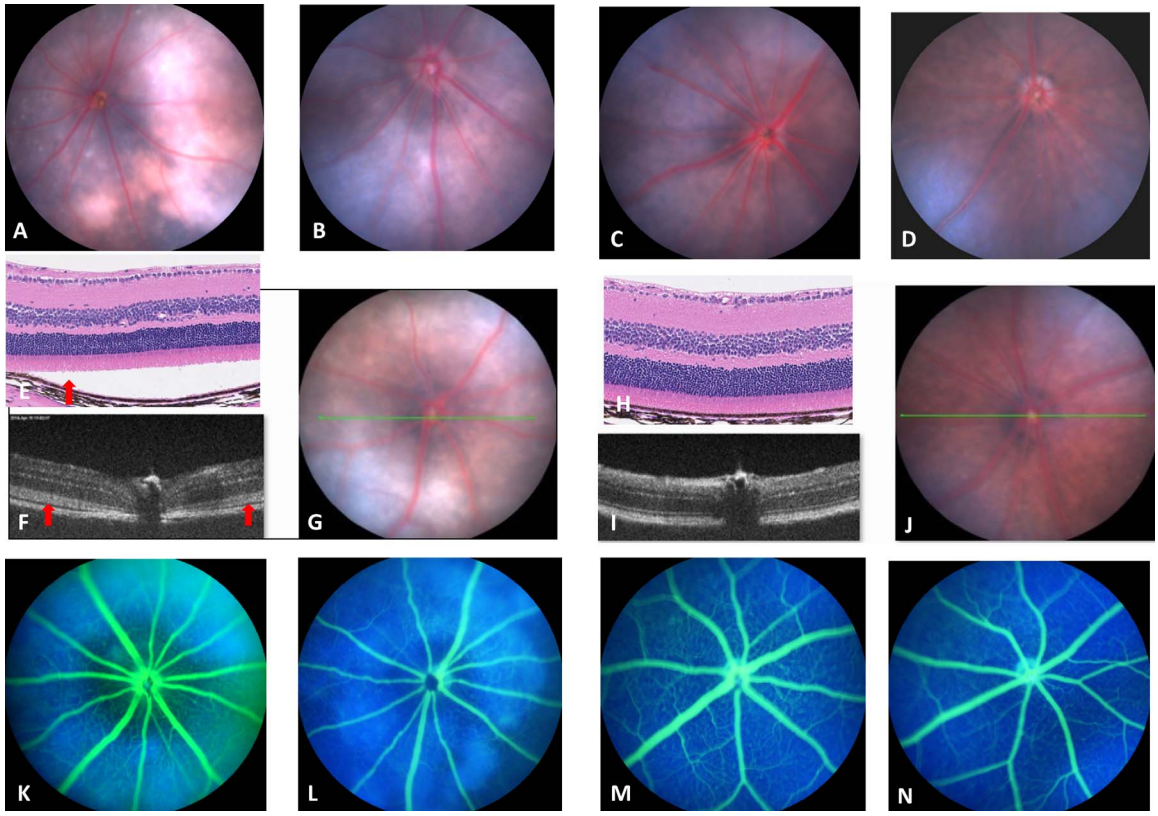

Figure 2. The clinical retinal phenotype of B6.ABJ-*rpea1* homozygotes. (**A**) Areas of retinal discoloration are observable at 6 weeks of age and (**B**) progress to large confluent regions by 6 months of age. Normal retinal appearance of nonmutant mice at (**C**) 6 weeks and (**D**) 6 months of age. Retinal detachment detected by histology (**E**) and by image-guided OCT (**F**), indicated by *red arrows*, was correlated with a discolored retinal area in the fundus image. (**G**) The *green line* indicates the location of the B-scan at 3 months of age. Histology (**H**) and B-scan (**I**) of normal control mice with image-guided OCT (**J**) were apparent in nonmutant control mice at 3 months of age. Retinal vasculature as assessed by fluorescein angiography was not different in mutants at 8 (**K**) and 33 (**L**) weeks of age in comparison to age matched controls (**M**, **N**).

rd1 mutations, the RD and other ocular phenotypes are recapitulated. By 6 months of age, all B6.ABJ-*Prkcq*^{rpea1}*Pde6b*^{rd1}/BOC mice had enlarged eyes (Fig. 1F) compared with C57BL/6J mice at the same age (Fig. 1G). The retinal star (Fig. 1H) and a complete RD (Fig. 1I) are observable by 1 month of age by Micron III image-guided OCT. The eye size (Fig. 1J) and IOP (Fig. 1K) were measured in C57BL/6J (white bar) and B6.ABJ-*Prkcq*^{rpea1}*Pde6b*^{rd1}/BOC (black bar) at 3 months of age (six mutants and six control mice at same age). The pathologic reason for the enlarged eyes with high IOP is most likely the secondary pupillary block glaucoma.

Complete RD: A Result of Photoreceptor Degeneration

The ABJ/LeJ strain, on which *nm3342* occurred, is known to carry two other mutations: the asebia Jackson in the stearoyl-Coenzyme A desaturase 1 (*Scd1*$^{ab\text{-}J}$) gene and retinal degeneration 1 in the phosphodiesterase 6b (*Pde6b*^{rd1}) genes Although homozygous *Scd1*$^{ab\text{-}J}$ mice have not been reported to have a retinal phenotype, they do exhibit an abnormal meibomian gland morphology.[20] Mutations in *Pde6b*^{rd1} lead to an early-onset, rapid photoreceptor degeneration.[21,22]

We noted that when the *rd1* locus was removed from B6.ABJ-*rpea1; rd1* mice by selective backcrossing, the star-shaped pattern, indicative of a complete RD, was absent. Therefore, we tested whether the complete RD phenotype occurred specifically because of an interaction with *Pde6b*^{rd1} or if it was the result of a generalized loss of photoreceptors. B6.ABJ/LeJ-*rpea1/rpea1* mice were crossed to retinal degeneration 4 (*Rd4*) mice that have a relatively rapid photoreceptor degeneration phenotype caused by a disruption in *Gnb1*.[23] All mice that were double mutants had a star-shaped fundus pattern, and a complete RD was observed at approximately 1 month of age (data not shown). This indicates that photoreceptor loss contributes to the severity of the RD, regardless of the underlying cause of the photoreceptor degeneration. However, the *rpea1* mutation is both necessary and sufficient to cause the disease phenotype, as neither *Pde6b*^{rd1} nor *Rd4* mutant alone develop RDs.

Retinal Detachment and Other Retinal Defects Including RPE Atrophy in *rpea1* Mutants on the C57BL/6 Background

When the *nm3342* mutation was moved to the C57BL/6J (B6) genetic background, fundus examination of the mutants revealed a blotchy and spotted phenotype beginning at 6 weeks of age (Fig. 2A). At 6 months, larger confluent regions of discoloration were observable by indirect ophthalmoscopy and by fundus photodocumentation (Fig. 2B). The clinical retinal phenotype of B6.ABJ-*rpea1* homozygotes is easily distinguishable from age-matched controls with a normal retinal appearance at 6 weeks (Fig. 2C) and 6 months of age (Fig. 2D). Retinal detachment, detected by both histology (Fig. 2E) and image-guided OCT (Fig. 2F), was correlated with the reduced pigmentation observed in the fundus images (Fig. 2G) at 3 months of age. Histology (Fig. 2H), OCT (Fig. 2I), and

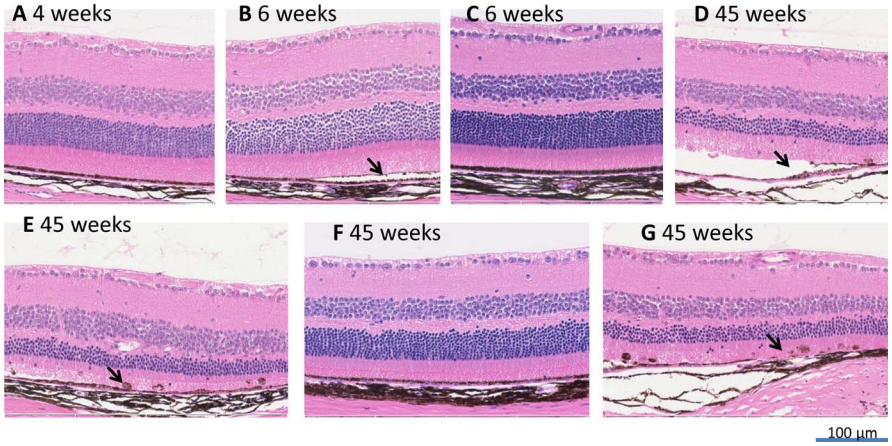

Figure 3. Histologic evaluation of B6.ABJ-*rpea1* demonstrating disease progression. Normal retinal histology is shown at 4 weeks of age (**A**). At 6 weeks of age, a focal area of retinal detachment ([**B**], *arrow*) is observed relative to the same age controls (**C**). Photoreceptor cell degeneration is evident both in the areas of detachment (**D**) and areas where detachment is not evident (**E**) at 45 weeks of age. Pigmented and nonpigmented nucleated cells are observed in the subretinal space ([**D**, **E**], *arrow*) compared with the same age control (**F**). Focal region of RPE atrophy observed at 45 weeks of age (**G**). *Scale bar*: 100 μm.

fundus images (Fig. 2J) of age-matched nonmutant control mice had a uniform color and appearance. Fluorescein angiography showed attenuated blood vessels in mutant animals at 6 months of age (Fig. 2L) in comparison to mutants at 2 months of age (Fig. 2K) and to age-matched controls (Figs. 2M, 2N). No fluorescein leakage was observed in mutants at either time points.

Hematoxylin and eosin–stained retinal sections of B6.ABJ-*rpea1* homozygous mutants showed a near normal retinal histology at 4 weeks of age (Fig. 3A). At 6 weeks of age, RD is apparent in mutants (Fig. 3B) compared with age-matched controls (Fig. 3C). Photoreceptor cell degeneration appeared to be pan-retinal as degeneration was evident in both areas of detachment (Fig. 3D), as well as normally attached regions (Fig. 3E). As mutants aged, pigmented and nonpigmented nucleated cells were frequently observed in the subretinal space (Figs. 3D, 3E), which were absent or rarely observed in age-matched controls (Fig. 3F). Focal areas of RPE atrophy were observed in mutants that were 45 weeks of age (Fig. 3G).

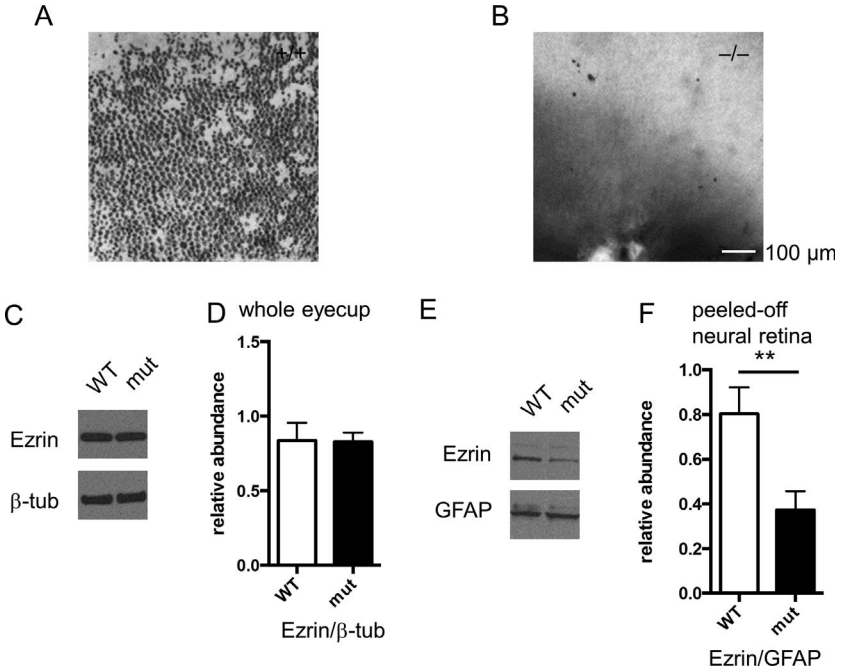

Figure 4. Decreased adhesion between RPE and photoreceptor outer segments of *Prkcq*$^{rpea1/rpea1}$ mice. Bright-field microscopy views of peeled-off retinas with exposed outer retinal surface harvested from (**A**) WT mice and (**B**) *Prkcq*$^{rpea1/rpea1}$ mice at 3 weeks old. *Scale bar*: 100 μm. (**C**) Western blot analysis showing similar ezrin level in WT and *Prkcq* mutant whole eyecup lysates. (**D**) Densitometric analysis of Western blots of ezrin normalized to β-tubulin, with results presented as arbitrary units (A.U.). (**E**) Western blot analysis showing reduced ezrin level in *Prkcq* mutant peeled-off neural retina lysates. (**F**) Densitometric analysis of Western blots of ezrin normalized to GFAP, with results presented as A.U. *Error bars* denote mean ± SD; $n = 3$ for each genotype. **Statistically significant ($P < 0.01$, unpaired *t*-test) difference between WT and mutant lysates.

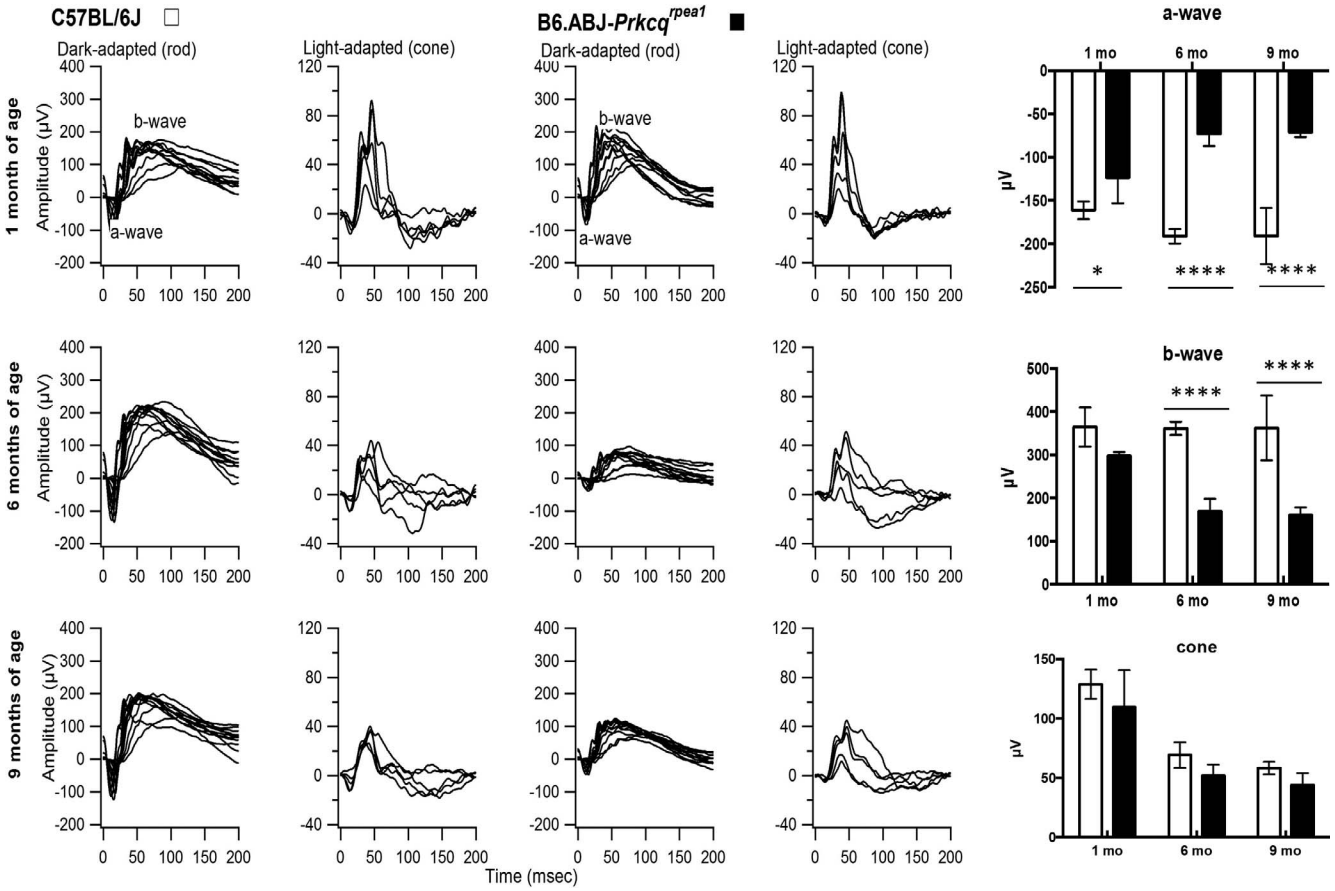

Figure 5. Electroretinograms of C57BL/6J and B6.ABJ-*rpea1* mutants at 1, 6, and 9 months of age. Dark-adapted responses were recorded after overnight dark adaptation, whereas light-adapted responses were recorded with a background light of 1.46 log cd/m^2 following a 10-minute exposure to the same intensity. Four eyes were tested for B6 and mutant mice at each age group. Results at 1 month of age: rod a-wave = −161.25 μV in B6 and −128.75 μV in mutant, *statistically significant at $P = 0.0435$; rod b-wave = 361.75 μV in B6 and 297.5 μV in mutant, not significant (NS); cone b-wave = 128.75 μV in B6 and 109.5 μV in mutant, NS. Results at 6 months of age: rod a-wave = −191.25 μV in B6 and −69.25 μV in mutant, ****statistically significant at $P < 0.0001$; rod b-wave = 361.75 μV in B6 and 168.75 μV in mutant, ****statistically significant at $P < 0.0001$; cone b-wave = 69.25 μV in B6 and 52.0 μV in mutant, NS. Results at 9 months of age: rod a-wave = −191.0 μV in B6 and −71.25 μV in mutant, ****statistically significant at $P < 0.0001$; rod b-wave = 362.5 μV in B6 and 160.25 μV in mutant, ****statistically significant at $P < 0.0001$; cone b-wave = 58.25 μV in B6 and 44.0 μV in mutant, NS.

The microvilli-rich apical domain of RPE interdigitates with the outer segment (OS) of photoreceptors. Nandrot et al.[19] use this physical interaction between the RPE microvilli and photoreceptor OS to assess the degree of retinal adhesion, by examining the melanin pigment of apical RPE cells that remains attached to the outer surface of the neural retina when it is peeled from the eyecup. We observed dense patches of RPE pigment on the outer surface of neural retina separated from the RPE in WT mice (Fig. 4A). In contrast, the separated neural retina from *rpea1* mice had dramatically fewer RPE pigments (Fig. 4B), indicating a reduced strength of adhesion between RPE and photoreceptor outer segments.

We next determined levels of RPE- and retina-specific proteins in lysates of whole eyecups and separated neural retinas (Figs. 4C–F). Glial fibrillary acidic protein levels were used as controls to assess recovery of neural retina, which were similar across samples (data not shown). Ezrin, a major protein of RPE apical microvilli, was found at equal levels in WT and mutant whole eyecups (Figs. 4C, 4D). In contrast, separated neural retina lysates of *rpea1* mutants showed reduced levels of ezrin compared with WT controls (Figs. 4E, 4F). Low levels of ezrin in neural retina extracts confirm the poor RPE–retina adhesion in PKCθ-deficient mice.

Aberrant ERG Phenotype in Homozygous B6.ABJ-*rpea1* Mutants

Electroretinograms of homozygous B6.ABJ-*rpea1* mice showed a slight decline beginning at 1 month of age (Fig. 5). By 6 months of age, mutants (black bar) showed a much-reduced rod ERG response, but the cone ERG responses were only slightly reduced compared with WT controls (white bar). The ERG responses were not significantly different in mutant mice at 9 months of age compared with that of mutants tested at 6 months of age (Fig. 5), suggesting the disease is stationary between 6 and 9 months. To examine the relative relationship of ERG responses to the rods and cones remaining in the retina, sections of eyes enucleated from the mice on which the ERGs were done were stained with rhodopsin, PNA, and cone opsins. The rod ERG changes appeared to be consistent with changes in ONL thickness and rhodopsin staining in the mutants, with minor changes at 1 month and significant losses by 6 months of age. Interestingly, PNA and blue opsin staining of the ventral retina were similar in mutant and WT; however, the dorsal cone matrix sheaths of *Prkcq* mutant were shorter than WT mice (Figs. 6F 6G, 6N, 6O). Also, the cone sheaths were shorter in regions of detachment compared with normally attached areas (Figs. 6L, 6M).

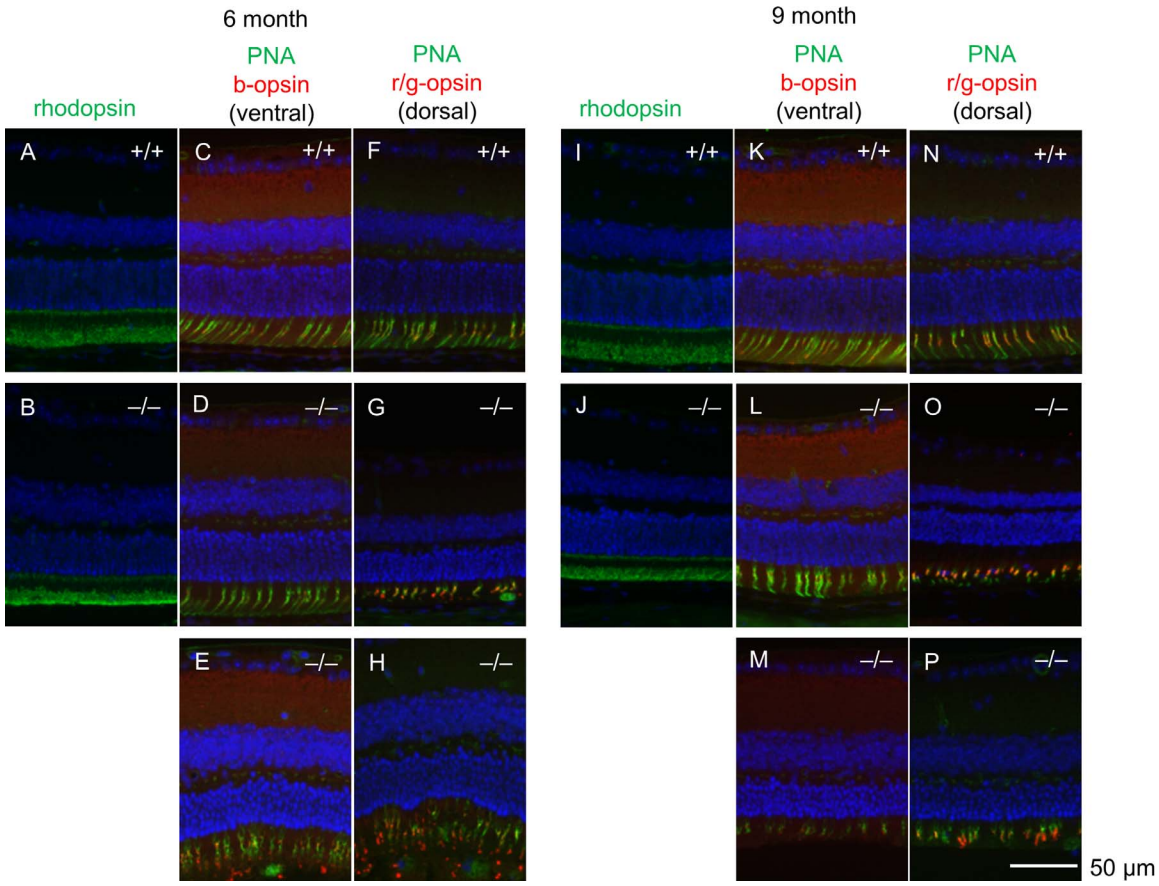

Figure 6. *Rpea1* mutant retinas display aberrant cone morphology. Immunohistochemical staining for rhodopsin showed thinning of the outersegments between WT (**A**, **I**) and mutants (**B**, **J**) at 6 months (**A**, **B**) and 9 months (**I**, **J**) old. Panels for PNA/blue-opsin staining were taken from ventral regions of WT (**C**, **K**) and mutant (**D**, **E**, **L**, **M**) retinas. Panels for PNA/red-opsin staining were taken from dorsal regions of WT (**F**, **N**) and mutant (**G**, **H**, **O**, **P**) retinas. **D**, **G**, **L**, and **O** represent normally attached regions of mutant retinas, whereas **E**, **H**, **M**, and **P** are areas of detachment. Retinas were harvested from 6- (**A**–**H**) and 9-month-old (**I**–**P**) mice. Rhodopsin (*green*), PNA (*green*), blue opsin (*red*), red/green opsin (*red*), DAPI (*blue*). *Scale bar*: 50 μm.

Mutation in *Prkcq* Is Identified in B6.ABJ-*rpea1* Homozygous Mutants

Through selective breeding, we were able to segregate *rpea1* from the *Scd1*$^{ab\text{-}J}$ mutation on chromosome 19 (Chr 19) and the *Pdeb*^{rd1} mutation on Chr 5. Genetic analysis indicated that the retinal phenotypes in homozygous B6.ABJ-*rpea1* mice were inherited as a single autosomal recessive mutation, and the *rpea1* mutation was mapped to mouse Chr 2 between microsatellite markers *D2Mit3* and *D2Mit360* (Fig. 7A). A genetic map of Chr 2 encompassing the *rpea1* locus, showing the closest markers, as well as the homologous region in humans, is depicted in Figure 7B.

A whole mouse exome capture library was prepared from DNA from a homozygous *rpea1* mouse and subjected to high-throughput sequencing. Within the critical interval in which the disease locus resided, two sequence changes with a high mismatch ratio were observed. The first was a nucleotide change from A to C in the *Itih5* gene. This nucleotide change had previously been reported as a SNP (*rs6269872*) among different strains and encodes a synonymous amino acid; therefore, it is unlikely to be the disease-causing locus. A second nucleotide change from a G to an A was found in the *Prkcq* gene. The base change (from GTAAG to GTAAA) occurs in the fifth base in intron 6 of the *Prkcq* gene (Fig. 7C), thereby potentially affecting the splice donor site. We sequenced the *Prkcq* cDNA in *rpea1* mice and found that, indeed, exon 6 was skipped (32-bp deletion in the cDNA sequence; Fig. 7D). The exon skipping creates a frameshift and premature stop codon (TG from exon 5 and A from exon 7—TGA) in the *Prkcq* transcript in *rpea1* mice (Fig. 7E). Western blot analysis with an anti-PKCθ antibody[24] showed an absence of protein in the *Prkcq*^{rpea1} mutant eye, suggesting that it is a null mutation (Fig. 7F).

Confirmation of the Causative Mutation in *rpea1*/*rpea1* Mice by Complementation Testing

A targeted mutant allele of *Prkcq* was generated 15 years ago[25] and cryopreserved at The Jackson Laboratory. B6.129P2-*Prkcq*^{tm1Litt}/J (stock #JR005711) mice were reanimated from the cryopreserved stock. Heterozygous *Prkcq*^{tm1Litt} mice, similar to *Prkcq*^{rpea1} heterozygous mice, show a normal retinal fundus appearance by photodocumentation and OCT (Supplementary Figs. S1A, S1B). Likewise, homozygous *Prkcq*^{tm1Litt} mice (Supplementary Figs. S1C, S1D) were similarly affected as homozygous *Prkcq*^{rpea1} mutants (Supplementary Figs. S1E, S1F) with RD and aberrant discoloration of the fundus. A complementation test between homozygous *Prkcq*^{tm1Litt} and homozygous *Prkcq*^{rpea1} mice confirmed that the spontaneous *rpea1* mutation was responsible for the observed retinal phenotypes (Supplementary Figs. S1G–S1J).

The B6.129P2-*Prkcq*^{tm1Litt}/J strain (stock #005711) carries the *Crb1*^{rd8} mutation, which was identified by genotype

Investigative Ophthalmology & Visual Science

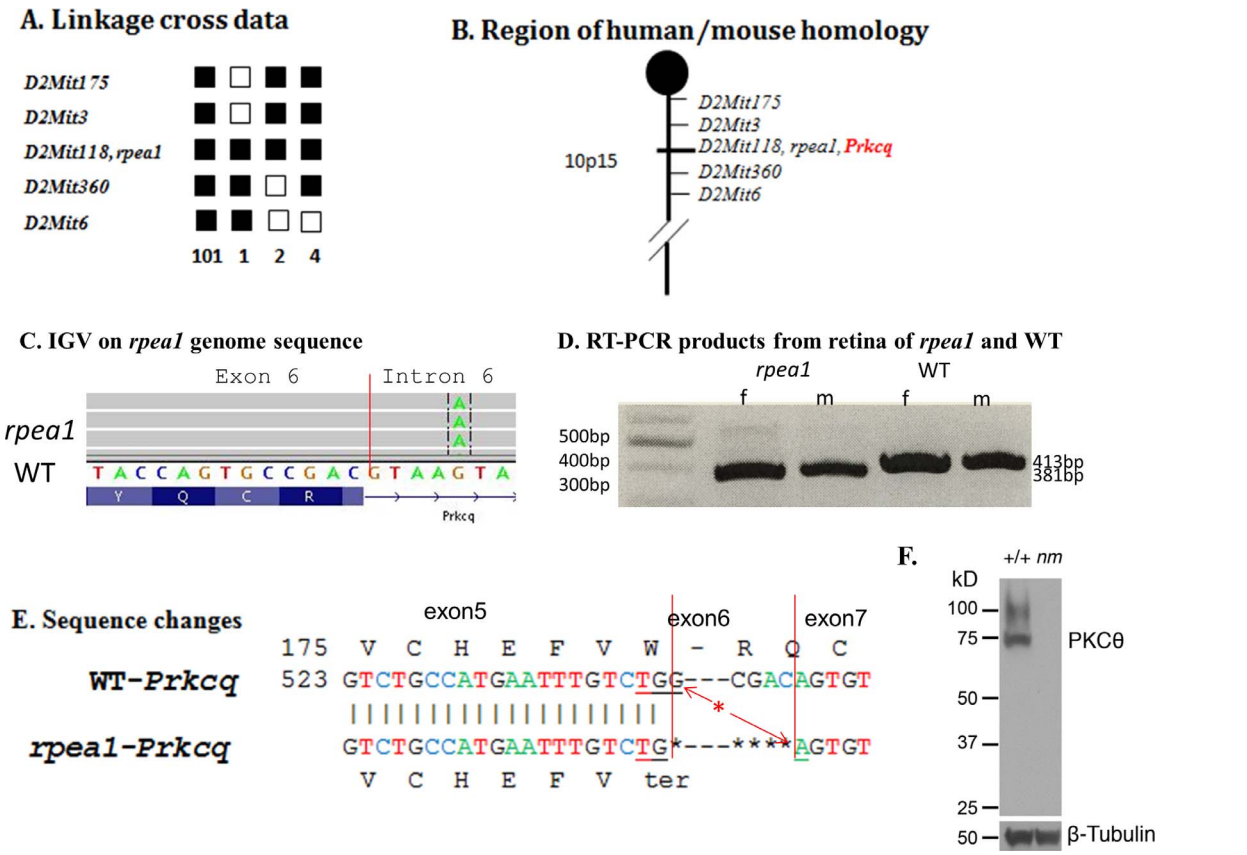

Figure 7. Genetic and molecular analysis of *rpea1/rpea1* mutants. (**A**) Fifty-four affected F2 progeny from an intercross between *rpea1/rpea1* and CAST/Ei mice were genotyped. Linkage to several markers on mouse Chr 2 was observed. The *columns of squares* represent haplotypes (*filled boxes*, *rpea1/rpea1* allele; *open boxes*, CAST/Ei allele). The number of chromosomes with each haplotype is indicated below each column. (**B**) Genetic map of Chr 2 in the *rpea1* region showing the closest markers and the region of human homology. (**C**) Integrative Genomics Viewer (IGV) shows the mismatch base. (**D**) Reverse transcriptase-PCR gel shows the *rpea1* homozygous female (f) and male (m) with a smaller band (381 bp) compared with WT controls (413 bp). (**E**) Sequence changes in *rpea1-Prkcq* compared with WT-*Prkcq*. (**F**) Western blot analysis for PKCθ in WT and *rpea1/rpea1* mutant (nm) whole eye lysates (20 μg protein per lane). β-Tubulin included as a loading control.

analysis.[26] Therefore, we outcrossed B6.129P2-*Prkcq*^{tm1Litt}/J mice to C57BL/6J and selected against the *Crb1*^{rd8} mutation. The retinal phenotypes of B6.129P2-*Prkcq*^{tm1Litt}/J (stock #028488) mice without *Crb1*^{rd8} (Supplementary Figs. S1K, S1L) did not differ from those of *rpea1* mutant mice.

PKCθ Is Enriched in the Lateral Plasma Membrane of RPE Cells

We determined by Western analysis that the PKCθ protein is highly enriched in RPE/choroid compared with that of retinal lysates (Fig. 8A). To further determine the regional and subcellular localization of the PKCθ protein, we performed immunofluorescence staining with an anti-PKCθ antibody on eye sections. Consistent with Western blot results, strong PKCθ signal was observed in the RPE layer. Specifically, PKCθ is present in the lateral surfaces of RPE cells (Fig. 8B). Due to strong nonspecific staining in the apical region of the RPE cells (Supplementary Fig. S2), we cannot exclude the possibility that PKCθ may be found at low levels in the apical RPE microvilli. PKCθ staining overlapped with that of ZO1 (TJP1), a tight junction protein, and β-catenin, an adherens junction protein in double-immunofluorescence analysis (Fig. 8C). The strong PKCθ localization in RPE cells suggests that the RD is likely to be caused by pathology or dysfunction in RPE cells. Similar localization of adherens junction proteins was observed in WT and *Prkcq* ^{rpea1} retinas at 16 days of age (Supplementary Fig. S3).

PKCθ Depletion Caused Abnormal Cortical F-Actin Organization and Elevated ERM Activity

Previous studies suggest that PKCθ may regulate the actin cytoskeleton by phosphorylating F-actin binding proteins in multiple cells types.[27] Indeed, phalloidin staining of filamentous actin (F-actin) in RPE flat mounts showed that, although F-actin forms compact perijunctional rings in the apical domain of WT RPE cells, both *Prkcq*^{rpea1} (Fig. 9B) and *Prkcq*^{tm1Litt} (data not shown) RPE cells displayed an unusual F-actin ring staining pattern. To determine whether the aberrant F-actin staining in PKCθ-deficient RPE cells was the result of increased levels of actin, Western blot analysis was performed on WT and *Prkcq* ^{rpea1} RPE/choroid lysates. No quantitative difference in the amount of total actin was observed between mutant and WT lysates (Fig. 9C).

To test whether the aberrant F-actin staining might be due to defects in linkage of F-actin to the apical domain, the activation status of ERM proteins, which link membrane-associated proteins to actin filaments at the cell cortex, was examined. Normally, phosphorylation of the C-terminal threonine (Thr567 of ezrin, Thr564 of radixin, Thr558 of moesin) of ERM proteins disrupts the self-inhibitory interaction between their N- and C-terminal domains, thus exposing the putative

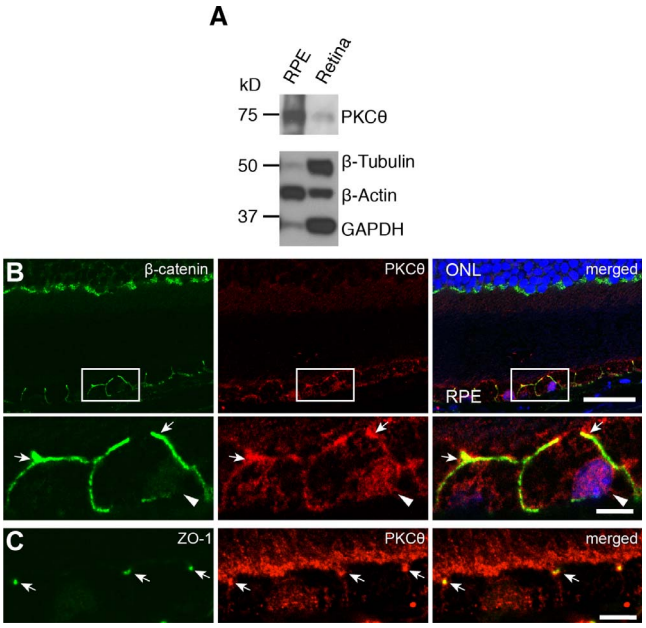

Figure 8. Localization of PKCθ in the eye and the RPE. (**A**) Western blot analysis for PKCθ showed relative enrichment of the protein in RPE/choroid lysates compared with the neural retina fraction (2 μg protein loaded per lane) in the WT mouse. (**B**) Immunofluorescence staining for PKCθ on WT eye sections showing strong staining in the RPE layer (*Upper*). (*Lower*) Colocalization (*arrows*) of PKCθ with the adherens junction protein β-catenin shown below at higher magnification. *Arrowheads* point to nuclei. (**C**) Colocalization (*arrows*) of PKCθ with the tight junction protein ZO-1. Note, the broad diffuse staining by anti-PKCθ of the apical RPE is nonspecific as *Prkcq1*^{rpea1} incubated with the primary antibody showed the same pattern of staining (Supplementary Fig. S2). *Scale bars*: 30 μm ([**B**], *Upper panel*); 5 μm ([**B**], *Lower panel*; [**C**], *panel*).

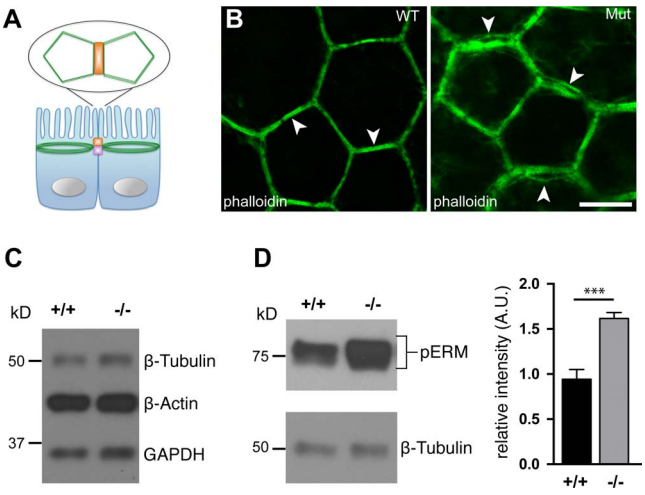

Figure 9. Loss of PKCθ leads to aberrant cortical F-actin in RPE cells from homozygous *Prkcq*^{rpea1} mutants. (**A**) Schematic depicting the apical F-actin ring structure. (**B**) Altered perijunctional F-actin staining (*arrowheads*) in postnatal (P)16 *Prkcq*^{rpea1} mutants. (**C**) Western blot analysis for β-tubulin, β-actin, and GAPDH showed no obvious difference in β-actin levels between WT (+/+) and *Prkcq* mutant (–/–) RPE/choroid lysates, with β-tubulin and GAPDH used as loading controls. (**D**) (*Left*) Western blot analysis for phosphor-ERM (pERM) showed increased protein levels in *Prkcq*^{rpea1} mutants (–/–) compared with WT (+/+) RPE/choroid lysates. (*Right*) Densitometric analysis of Western blots of pERM normalized to β-tubulin, with results presented as A.U. *Error bars* denote mean ± SD (WT, 0.92 ± 0.12; *Prkcq*^{rpea1} mutant, 1.64 ± 0.06; $n = 3$ for each genotype). ***Statistically significant ($P = 0.0009$, unpaired *t*-test) differences between WT and mutant lysates. *Scale bar*: 20 μm.

actin-binding domain. Among the many kinases that have been shown to phosphorylate this conserved threonine, PKCθ was identified as a major kinase that phosphorylated Thr558 of moesin.[28] Western blot analysis of RPE/choroid lysates showed that in the absence of PKCθ activity, the active phospho-ezrin (Thr567)/radixin (Thr564)/moesin (Thr558) levels were increased (Fig. 9D), whereas the expression levels of total ERM proteins were not affected (Supplementary Figs. S4A, S4F). This indicates that PKC is unlikely to be the kinase that is responsible for the phosphorylation of ERM threonine residues in RPE cells in vivo but must affect ERM in an indirect fashion, potentially by negatively regulating the phosphorylation and activation of the ERMs. It is also interesting to note that staining of the microvilli for ERM was similar between WT (Supplementary Figs. S4B, S4C, S4G, S4I, S4K) and mutants (Supplementary Figs. S4D, S4E, S4H, S4J, S4L), suggesting that the apical microvilli are not affected by the PKCθ deficiency.

Discussion

Retinal detachment, a pathology associated with many different eye diseases, can lead to serious consequences, including blindness. Much work has been done to understand the consequences of induced RD in animal models. Subretinal injection of sodium hyaluronate is a widely accepted method for inducing retinal detachment,[29] and the oxygen-induced retinopathy (OIR) model recapitulates some of the disease phenotypes associated with detachment caused in human infants with retinopathy of prematurity.[30] Study of both model systems has allowed for insight into the pathologic consequences of RD and associated molecular mechanisms. However, these approaches can be technically challenging with variable outcome and not be entirely representative of the human condition, for example, in the timing of disease initiation during development.[30]

In this study, we describe a robust, heritable model of exudative retinal detachment that is caused by a disruption in the *Prkcq* gene. A previous publication showing neuroretinal localization of PKCθ that varied depending on the age, disease state, and antibody used. Additionally, elevated *Pkcq* mRNA and protein levels in *Pde6b*^{rd1} P11 mutants relative to controls suggested that PKCθ might potentially play a role in the retina.[31] Thus far, a role for PKCθ in the eye has not been confirmed, and this is the first report to show that PKCθ deficiency leads to exudative RD and late-onset RPE atrophy. Our results suggest that the RD phenotype is likely to result from defective RPE function, as PKCθ is expressed predominantly in RPE/choroid tissue and only at low levels in the retina of the mouse eye. The PKCθ deficiency causes dramatic reorganization of F-actin in RPE cells, indicating the importance of novel isoforms of PKC in the regulation of F-actin organization in epithelial cells.

PKCθ is a non–calcium-dependent member of the serine- and threonine-specific protein kinase family that is activated by the second messenger diacylglycerol. Previous studies have shown that PKCθ may affect barrier function through phosphorylation of junctional proteins that are critical for selective epithelial permeability.[32,33] For example, PKCθ has been shown to affect barrier permeability of intestinal epithelium by modulation of claudins. Also, PKCθ and/or PKCδ have been reported to enhance barrier function of the nasal epithelium through the up-regulation of tight junction

Investigative Ophthalmology & Visual Science

proteins via the transcriptional factor GATA3.[32] The actin cytoskeleton, especially the perijunctional actin ring, which is abnormal in *Prkcq*^{rpea1} mutants, plays an important role in maintaining the barrier function of epithelial cells as well.[34] In addition to a role in epithelial cells, PKCθ may have similar functions in endothelial cells. In an in vitro rat endothelial capillary system, PKCθ was shown to be essential for processes associated with angiogenesis and wound repair, including endothelial mitosis, maintenance of the actin cytoskeleton, and formation of an enclosed tub.[35] Therefore, we hypothesize that the mutation in PKCθ is likely to cause the RD phenotype through its effects on RPE barrier function.

The aberrant F-actin perijunctional ring observed in RPE cells from *Prkcq*^{rpea1} mutants was not due to an overexpression of total actin, but may in part be caused by the elevated levels of activated ERM proteins that, in their phosphylated state, link F-actin with the plasma membrane. Although in leukocytes, PKCθ was reported to phosphorylate the conserved threonine residue necessary for activation of ERMs,[28] we actually observed an increase in phosphorylation of the ERMs in *Prkcq*^{rpea1} mutants, which are deficient in PKCθ. Perhaps, under normal circumstances, PKCθ functions in an indirect fashion to inhibit a downstream molecule or pathway that in turn regulate ERMs in RPE/endothelial cells. Multiple kinases have been shown to phosphorylate the conserved threonine of ERM proteins in various cell types, including Rho kinase,[36] NIK (NF-κB–inducing kinase),[37] and LOK (lymphocyte-oriented kinase).[38] Alternatively, PKCθ may activate a phosphatase that normally dephosphorylates ERM proteins, much as the hematopoietic protein tyrosine phosphatase is activated by PKCθ in the immune synapse.[39] Careful study of the B6.ABJ-*Prkcq*^{rpea1} and B6.129P2-*Prkcq*^{tm1Litt}/J mutants is likely to reveal the mechanisms and pathways that are important in maintaining proper fluid homeostasis in the posterior retina.

Acknowledgments

The authors thank Mark P. Krebs and Jürgen K. Naggert for careful review of the manuscript. Supported by National Institutes of Health Grants R01 EY019943 (BC), R01 EY016501 (PMN), and P30 CA034196 (The Jackson Laboratory Shared Services); the Macular Vision Research Foundation; and The Edward N. & Della L. Thome Memorial Foundation.

Disclosure: **X. Ji**, None; **Y. Liu**, None; **R. Hurd**, None; **J. Wang**, None; **B. Fitzmaurice**, None; **P.M. Nishina**, None; **B. Chang**, None

References

1. Vilaplana F, Muinos SJ, Nadal J, Elizalde J, Mojal S. Stickler syndrome. Epidemiology of retinal detachment. *Arch Soc Espanola Oftalmol*. 2015;407:1433–1449.
2. Vigil-De Gracia P, Ortega-Paz L. Retinal detachment in association with pre-eclampsia, eclampsia, and HELLP syndrome. *Int J Gynaecol Obstetrics*. 2011;114:223–225.
3. Holden B, Sankaridurg P, Smith E, Aller T, Jong M, He M. Myopia, an underrated global challenge to vision: where the current data takes us on myopia control. *Eye*. 2014;28:142–146.
4. Saint-Geniez M, D'Amore PA. Development and pathology of the hyaloid, choroidal and retinal vasculature. *Int J Dev Biol*. 2004;48:1045–1058.
5. Spencer WH (ed.). *Ophthalmic Pathology: An Atlas and Textbook*. 4th ed. Philadelphia: W.B. Saunders Company; 1996.
6. Nentwich MM, Ulbig MW. Diabetic retinopathy: ocular complications of diabetes mellitus. *World J Diabetes*. 2015;6:489–499.
7. Yagi F, Takagi S, Tomita G. Incidence and causes of iatrogenic retinal breaks in idiopathic macular hole and epiretinal membrane. *Semin Ophthalmol*. 2014;29:66–69.
8. Mitry D, Charteris DG, Fleck BW, Campbell H, Singh J. The epidemiology of rhegmatogenous retinal detachment: geographical variation and clinical associations. *Br J Ophthalmol*. 2010;94:678–684.
9. Kaur C, Foulds WS, Ling EA. Blood-retinal barrier in hypoxic ischaemic conditions: basic concepts, clinical features and management. *Prog Retin Eye Res*. 2008;27:622–647.
10. Marmor MF, Yao XY. Conditions necessary for the formation of serous detachment. Experimental evidence from the cat. *Arch Ophthalmol*. 1994;112:830–838.
11. Dustin ML. PKC-theta: hitting the bull's eye. *Nat Immunol*. 2011;12:1031–1032.
12. Bertram A, Zhang H, von Vietinghoff S, et al. Protein kinase C-theta is required for murine neutrophil recruitment and adhesion strengthening under flow. *J Immunol*. 2012;188:4043–4051.
13. Madaro L, Marrocco V, Fiore P, et al. PKCtheta signaling is required for myoblast fusion by regulating the expression of caveolin-3 and beta1D integrin upstream focal adhesion kinase. *Mol Biol Cell*. 2011;22:1409–1419.
14. Hawes NL, Smith RS, Chang B, Davisson M, Heckenlively JR, John SW. Mouse fundus photography and angiography: a catalogue of normal and mutant phenotypes. *Mol Vis*. 1999;5:22.
15. Chang B, Hawes NL, Pardue MT, et al. Two mouse retinal degenerations caused by missense mutations in the beta-subunit of rod cGMP phosphodiesterase gene. *Vision Res*. 2007;47:624–633.
16. Truett GE, Heeger P, Mynatt RL, Truett AA, Walker JA, Warman ML. Preparation of PCR-quality mouse genomic DNA with hot sodium hydroxide and tris (HotSHOT). *Biotechniques*. 2000;29:52–54.
17. Taylor BA, Navin A, Phillips SJ. PCR-amplification of simple sequence repeat variants from pooled DNA samples for rapidly mapping new mutations of the mouse. *Genomics*. 1994;21:626–632.
18. Fairfield H, Gilbert GJ, Barter M, et al. Mutation discovery in mice by whole exome sequencing. *Genome Biol*. 2011;12:R86.
19. Nandrot EF, Anand M, Sircar M, Finnemann SC. Novel role for alphavbeta5-integrin in retinal adhesion and its diurnal peak. *Am J Physiol Cell Physiol*. 2006;290:C1256–C1262.
20. Sundberg JP, Boggess D, Sundberg BA, et al. Asebia-2J (Scd1(ab2J)): a new allele and a model for scarring alopecia. *Am J Pathol*. 2000;156:2067–2075.
21. Keeler C. Retinal degeneration in the mouse is rodless retina. *J Hered*. 1966;57:47–50.
22. Bowes C, Li T, Danciger M, Baxter LC, Applebury ML, Farber DB. Retinal degeneration in the rd mouse is caused by a defect in the beta subunit of rod cGMP-phosphodiesterase. *Nature*. 1990;347:677–680.
23. Roderick TH, Chang B, Hawes N, Heckenlively J. A new dominant retinal degeneration (*Rd4*) associated with a chromosomal inversion in the mouse. *Genomics*. 1997;42:393–396.
24. Poole DP, Van Nguyen T, Kawai M, Furness JB. Protein kinases expressed by interstitial cells of Cajal. *Histochem Cell Biol*. 2004;121:21–30.
25. Sun Z, Arendt CW, Ellmeier W, et al. PKC-theta is required for TCR-induced NF-kappaB activation in mature but not immature T lymphocytes. *Nature*. 2000;404:402–407.
26. Chang B, Hurd R, Wang J, Nishina P. Survey of common eye diseases in laboratory mouse strains. *Invest Ophthalmol Vis Sci*. 2013;54:4974–4981.

27. Larsson C. Protein kinase C and the regulation of the actin cytoskeleton. *Cell Signal*. 2006;18:276–284.
28. Pietromonaco SF, Simons PC, Altman A, Elias L. Protein kinase C-theta phosphorylation of moesin in the actin-binding sequence. *J Biol Chem*. 1998;273:7594–7603.
29. Matsumoto H, Miller JW, Vavvas DG. Retinal detachment model in rodents by subretinal injection of sodium hyaluronate. *J Vis Exp*. 2013;79:50660.
30. Hartnett ME. Pathophysiology and mechanisms of severe retinopathy of prematurity. *Ophthalmology*. 2015;122:200–210.
31. Azadi S, Paquet-Durand F, Medstrand P, van Veen T, Ekström PA. Up-regulation and increased phosphorylation of protein kinase C (PKC) delta, mu and theta in the degenerating rd1 mouse retina. *Mol Cell Neurosci*. 2006;31:759–773.
32. Koizumi J, Kojima T, Ogasawara N, et al. Protein kinase C enhances tight junction barrier function of human nasal epithelial cells in primary culture by transcriptional regulation. *Mol Pharmacol*. 2008;74:432–442.
33. Willis CL, Meske DS, Davis TP. Protein kinase C activation modulates reversible increase in cortical blood-brain barrier permeability and tight junction protein expression during hypoxia and posthypoxic reoxygenation. *J Cerebral Blood Flow Metab*. 2010;30:1847–1859.
34. Beryozkin A, Zelinger L, Bandah-Rozenfeld D, et al. Identification of mutations causing inherited retinal degenerations in the Israeli and Palestinian populations using homozygosity mapping. *Invest Ophthalmol Vis Sci*. 2014;55:1149–1160.
35. Tang S, Morgan KG, Parker C, Ware JA. Requirement for protein kinase C theta for cell cycle progression and formation of actin stress fibers and filopodia in vascular endothelial cells. *J Biol Chem*. 1997;272:28704–28711.
36. Zhang C, Wu Y, Xuan Z, et al. p38MAPK, Rho/ROCK and PKC pathways are involved in influenza-induced cytoskeletal rearrangement and hyperpermeability in PMVEC via phosphorylating ERM. *Virus Res*. 2014;192:6–15.
37. Baumgartner M, Sillman AL, Blackwood EM, et al. The Nck-interacting kinase phosphorylates ERM proteins for formation of lamellipodium by growth factors. *Proc Natl Acad Sci U S A*. 2006;103:13391–13396.
38. Belkina NV, Liu Y, Hao JJ, Karasuyama H, Shaw S. LOK is a major ERM kinase in resting lymphocytes and regulates cytoskeletal rearrangement through ERM phosphorylation. *Proc Natl Acad Sci U S A*. 2009;106:4707–4712.
39. Nika K, Charvet C, Williams S, et al. Lipid raft targeting of hematopoietic protein tyrosine phosphatase by protein kinase C theta-mediated phosphorylation. *Mol Cell Biol*. 2006;26:1806–1816.

Investigative Ophthalmology & Visual Science